J|A|C|S
ARTICLES
Published on Web 05/12/2007

# Probing Excitation Delocalization in Supramolecular Chiral Stacks by Means of Circularly Polarized Light: Experiment and Modeling

Frank C. Spano,*,† Stefan C. J. Meskers,*,‡ Emanuelle Hennebicq,§ and David Beljonne§

*Contribution from the Department of Chemistry, Temple University, Beury Hall 201, Philadelphia, Pennsylvania 19122, Laboratory of Macromolecular and Organic Chemistry, Eindhoven University of Technology, P.O. Box 513, 5600 MB Eindhoven, The Netherlands, and Chemistry of Novel Materials, University of Mons-Hainaut, Place du Parc 20, B-7000 Mons, Belgium*

Received October 12, 2006; E-mail: spano@temple.edu; s.c.j.meskers@tue.nl

***Abstract:*** Photoexcitations in helical aggregates of a functionalized, chiral oligophenylenevinylene (MOPV) are described going beyond the Born−Oppenheimer approximation, in the form of dressed (polaronic) Frenkel excitons. This allows for accurate modeling of the experimentally observed wavelength dependence of the circular polarization in fluorescence, which directly probes the non-adiabatic nature of the electron-vibration (EV) coupling in this system. The fluorescence photon is emitted from a nuclear geometry in which one MOPV and its two nearest neighbors have a nuclear equilibrium that differs appreciably from the ground state due to the presence of the excited state. The absorption and emission band shape and the circular dichroism are consistent with a coherence range of the emitting excitation of approximately two neighboring molecules. Random fluctuations in the zero-order excited-state energy of the MOPVs (disorder) limit the exciton delocalization and can be described by a Gaussian distribution of energies with a width $\sigma = 0.12$ eV and a spatial correlation length $l_0 \approx 5$ molecules. We find that disorder and EV coupling act synergistically in localizing the emitting exciton to a single MOPV in the aggregate with 95% probability.

## I. Introduction

The photophysical behavior of organic multi-chromophoric systems, from artificial systems such as thin polymeric films used in field effect transistors and solar cells to biological systems best exemplified by photosynthetic antennas, has been the subject of numerous investigations. Whether considering energy or charge transport, all of these diverse systems share a common feature that sets them apart from the typical inorganic semiconductors: they are "soft" in the sense that transport is accompanied by significant nuclear distortion induced by nonadiabatic electron-vibrational coupling. The resulting increase in the effective mass (and reduction in the bandwidth of the excitation) makes organic systems far more susceptible to the localizing effects of disorder. In our view, the major challenge in properly understanding charge and energy transport in organic materials lies in a detailed understanding of the coupling between electronic excitations and the nuclear framework over which they travel. This requires a quantum mechanical description, going beyond the usual Born−Oppenheimer approximation and experimental techniques that are sensitive to the nonadiabaticity in the electron-vibrational coupling.

Very promising candidates for the study of soft excitations in organic condensed phase materials are the well-characterized $\pi$-stacked helical aggregates of substituted chiral oligophenylenes (MOPVn, see Figure 1), which form in low-temperature solution.[1−6] The rungs of the helix are formed from two OPVn chromophores quadruple hydrogen-bonded through triazine head groups. Such well-defined supramolecular architectures, besides being of potential interest for applications in electronics and photonics, are ideal systems for testing theoretical models of energy transport. In addition to (unpolarized) absorption and emission, these systems are amenable to circular dichroism (CD) and circularly polarized luminescence (CPL) spectroscopies.[7−9] An interesting feature often observed for these aggregates is that the isolated constituent chromophoric molecules do not show any significant circular polarization, in contrast to the

† Temple University.
‡ Eindhoven University of Technology.
§ University Mons-Hainaut.

(1) Schenning, A. P. H. J.; Jonkheijm, P.; Peeters, E.; Meijer, E. W. *J. Am. Chem. Soc.* **2001**, *123*, 409−416.
(2) Jonkheijm, P.; Hoeben, F. J. M.; Kleppinger, R.; Van Herrikhuyzen, J.; Schenning, A. P. H. J.; Meijer, E. W. *J. Am. Chem. Soc.* **2003**, *125*, 15941−15949.
(3) Hoeben, F. J. M.; Herz, L. M.; Daniel, C.; Jonkheijm, P.; Schenning, A. P. H. J.; Silva, C.; Meskers, S. C. J.; Beljonne, D.; Phillips, R. T.; Friend, R. H.; Meijer, E. W. *Angew. Chem., Int. Ed.* **2004**, *43*, 1976−1979.
(4) Prins, P.; Senthilkumar, K.; Grozema, F. C.; Jonkheijm, P.; Schenning, A. P. H. J.; Meijer, E. W.; Siebbeles, L. D. A. *J. Phys. Chem. B.* **2005**, *109*, 18267−18274.
(5) Jeukens, C.; Jonkheijm, P.; Wijnen, F. J. P.; Gielen, J. C.; Christianen, P. C. M.; Schenning, A. P. H. J.; Meijer, E. W.; Maan, J. C. *J. Am. Chem. Soc.* **2005**, *127*, 8280−8281.
(6) Jonkheijm, P.; van der Schoot, P.; Schenning, A. P. H. J.; Meijer, E. W. *Science* **2006**, *313*, 80−83.
(7) *Circular Dichroism Principles and Applications*; Nakanishi, K., Berova, N., Woody, R. W., Eds.; Wiley-VCH: New York, 2000.

 **10.1021/ja067321g CCC: $37.00** 

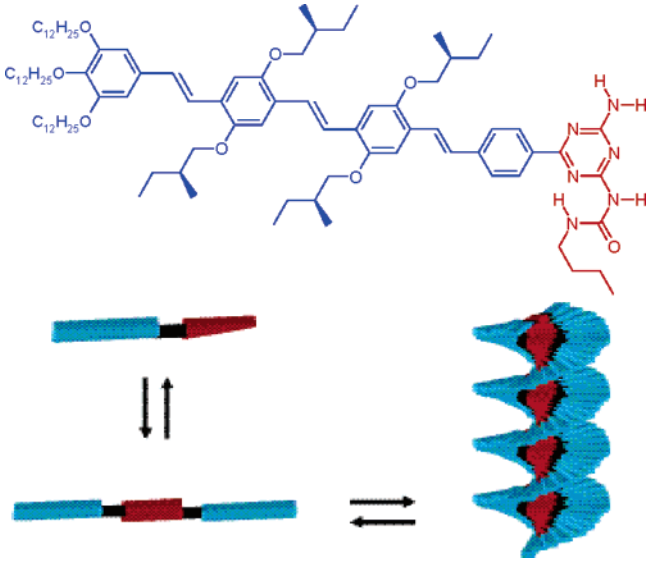

***Figure 1.*** Assembly of MOPV4 chiral aggregate through H-bonded dimer intermediates.

aggregate where circular differentials can be very large.[1−3,10−12] This observation has been explained using the exciton chirality model. Here the circular polarization arises from delocalization of the optical excitation over two or more achiral chromophoric units which are held in a helical arrangement either by supramolecular forces or by a scaffold.[13] The sensitivity of the circular polarization for delocalization of the optical excitation[14] makes circular polarization measurements ideal for studying the behavior of excitations in multi-chromophoric systems.

A proper accounting of the four photophysical observables under study here, absorption band shape, emission band shape, and circular polarization in absorption and emission, provides a strict test for any quantum mechanical model for photoexcitations in molecular aggregates. In the present case, we subject the Holstein Hamiltonian with site-correlated disorder, recently introduced to successfully interpret absorption and emission in P3HT thin films,[15] to the task of describing the nature of the optical excitations in MOPV4 helical aggregates. For weakly coupled chromophores, such excitations are essentially vibronic excitons in which an electronic excitation on a given molecule relaxes along a given nuclear coordinate. For MOPV4 (as well as most conjugated molecules), the nuclear coordinate corresponds to the strongly coupled intramolecular ring-breathing/vinyl stretching mode with frequency $\sim$1400 cm$^{-1}$. This mode forms clear vibronic progressions in the absorption and emission spectra of single molecules in solution. Moreover, in an aggregate, even the surrounding molecules will relax or "bend" in response to the vibronic excitation. Such processes are accounted for by supplementing the vibronic basis set (aka single particle basis set) with two-particle basis functions composed of vibronic/vibrational pairs.[16,17] Hence, optical excitations in organic systems can be described as delocalized vibronic excitations surrounded by vibrational or phonon clouds. The vibronic component is the primary source of the unpolarized absorption and CD spectra, whereas the vibronic/vibrational pairs play an essential role in the emission process.

We have previously shown that the degree of circular polarization ($g_{lum} = 2(I_L - I_R)/(I_L + I_R)$ with $I_{L(R)}$ being the intensity of left (right) circular polarized luminescence) in the sideband luminescence arises from two-particle excitations.[18] Hence, $g_{lum}(\omega)$ probes the size of the phonon cloud. A complete analysis of the four observables allows one to construct in some detail the fundamental optical excitations in MOPV4 helices, which can be referred to as neutral polarons. The overall analysis is general enough to treat other chiral condensed phase organic systems, such as chiral polythiophene aggregates and even DNA.

Delocalization of the excitations over a large number of molecules can give rise to unexpected phenomena such as superradiance,[19,20] but delocalization is often strongly influenced by the energetic disorder, i.e., the fact that not all chromophoric units have exactly the same excitation energy. In a previous work, we have investigated the dynamics of energy diffusion along MOPV4 chiral stacks via free excitons (uncoupled to nuclear degrees of freedom) and found that the measured emission depolarization can only be reproduced by accounting for excitation delocalization among acceptor molecules, assuming complete localization over a single donor chromophore after geometric relaxation.[21] Here, we aim at quantifying further the nature of the absorbing and emitting excitons. A proper characterization requires not only the extent (and shape) of the nuclear distortion field accompanying the polaron but also its coherence range. Both parameters are affected by disorder, presenting a rather formidable challenge in formulating a valid theoretical description. However, in recent years, numerical procedures for the analysis of the Holstein Hamiltonian with disorder have been developed and applied to herringbone assemblies of conjugated oligomers[17,22] as well as linear $\pi$-stacks of polythiophenes.[15] In the present paper, we utilize these methods to extend our work on chiral aggregates[18] to include the effects of a Gaussian distribution of correlated site disorder.

## II. The Disordered Holstein Model

The equilibrium aggregate structure for MOPV4 shown in Figure 1 is based on molecular mechanics calculations using the Dreiding force field.[23] The angle $\phi$ between neighboring superimposed chromophores is of the order of 10°. Simulations of energy transfer along the stacks[21] show that excellent agreement with experiment is obtained for angles in the range 6−12°. According to the force field calculations, the intermo-


(8) Langeveld-Voss, B. M. W.; Janssen, R. A. J.; Christiaans, M. P. T.; Meskers, S. C. J.; Dekkers, H. P. J. M.; Meijer, E. W. *J. Am. Chem. Soc.* **1996**, *118*, 4908−4909.
(9) Peeters, E.; Ramos, A. M.; Meskers, S. C. J.; Janssen, R. A. J. *J. Chem. Phys.* **2000**, *112*, 9445−9454.
(10) Wang, M. M.; Silva, G. L.; Armitage, B. A. *J. Am. Chem. Soc.* **2000**, *122*, 9977−9986.
(11) DeRossi, U.; Dähne, S.; Meskers, S. C. J.; Dekkers, H. P. J. M. *Angew. Chem., Int. Ed.* **1996**, *35*, 760−763.
(12) Spitz, C.; Dähne, S.; Ouart, A.; Abraham, H. W. *J. Phys. Chem. B.* **2000**, *104*, 8664−8669.
(13) Harada, N.; Nakanishi, K. *Circular Dichroic Spectroscopy*; Oxford: New York, 1983.
(14) Didraga, C.; Knoester, J. *J. Chem. Phys.* **2004**, *121*, 10687−10698.
(15) Spano, F. C. *J. Chem. Phys.* **2005**, *122*, 234701/1−15; erratum **2007**, *126*, 159901.
(16) Philpott, M. R. *J. Chem. Phys.* **1971**, *55*, 2039−2054.
(17) Spano, F. C. *J. Chem. Phys.* **2002**, *116*, 5877−5891.
(18) Spano, F. C.; Zhao, Z.; Meskers, S. C. J. *J. Chem. Phys.* **2004**, *120*, 10594−10604.
(19) Spano, F. C. *Chem. Phys. Lett.* **2000**, *331*, 7−13.
(20) Meinardi, F.; Cerminara, M.; Sassella, A.; Bonifacio, R.; Tubino, R. *Phys. Rev. Lett.* **2003**, *91*, 247401−247404.
(21) Beljonne, D.; Hennebicq, E.; Daniel, C.; Herz, L. M.; Silva, C.; Scholes, G. D.; Hoeben, F. J. M.; Jonkheijm, P.; Schenning, A. P. H. J.; Meskers, S. C. J.; Phillips, R. T.; Friend, R. H.; Meijer, E. W. *J. Phys. Chem. B* **2005**, *109*, 10594−10604.
(22) Spano, F. C. *Ann. Rev. Phys. Chem.* **2006**, *57*, 217−243.

lecular separation between adjacent H-bonded dimers along the stacks is 3.75 Å.

For the aggregates considered here, the exciton coupling, $J_{mn}$ between molecule $m$ and $n$, is evaluated by combining a coupled cluster single and double (CCSD) approach to the INDO Hamiltonian on the basis of model geometric structures, see ref 21. Transition charge densities are calculated for each chromophore $m$ and $n$ (in the gas phase), and the interaction $J_{mn}$ is evaluated via a Coulombic sum. The screening influence of intervening molecules, either MOPV or solvent, between $m$ and $n$ is neglected. As an illustration, the INDO/CCSD nearest neighbor interactions amount to ~0.057 [0.046] eV between superimposed molecules for a 6° [12°] rotation and only ~−0.0087 eV between chromophores belonging to the same H-bonded dimer. Hence, the intrastrand interactions are much larger than those between strands, suggesting an effective single strand approximation, as will be described below.

Note that, in contrast to ref 21 where coupling to a soft libration mode was inferred to rationalize the large Stokes shift observed for dissolved molecules, an almost perfect quantitative agreement to the measured optical properties of the aggregates is obtained here while only retaining an effective high-frequency mode. This can be explained by the fact that the conjugated backbones significantly planarize when they are incorporated in the helical stacks.

In addition to electronic coupling, there is significant electron-vibrational (EV) coupling within each helical stack due to the impact of various types of molecular motion on the excitonic couplings and site energies. To account for such effects, we treat EV coupling on two levels. At the most approximate level, we treat the conglomerate of acoustic and optical lattice modes with relatively low frequencies in the manner described by Schreiber and Toyazawa.[24] Here the overall effect of such lattice modes is to induce spatial and temporal fluctuations in the on-site excitation energy around the rigid lattice value. Under the adiabatic approximation, valid when the phonon energy is much less than the exciton bandwidth, the lattice coordinates are considered fixed during optical absorption or emission, resulting in a Gaussian distribution of spatially correlated site energies. Although spatial correlation was neglected by Schreiber and Toyozawa, we include it here within the model introduced by Knapp.[25] The variance of the site-energy distribution as well as the spatial correlation length are model parameters, which generally depend on temperature as well as the average phonon frequency and EV coupling constant. Alternatively, the distribution of site energies can arise from static point and structural defects. In this case, the distribution parameters do not depend on temperature. In this work, we do not distinguish between the two origins.

A more accurate treatment of EV coupling is reserved for the high-energy intramolecular symmetric stretching/breathing vibrational mode at ~1400 $cm^{-1}$, common to many molecules with extended $\pi$-conjugation. This mode causes a pronounced vibrational progression in both the absorption and emission spectra of oligo-pheneylene vinylene molecules in solution.[9,26,27] In this work, the 1400 $cm^{-1}$ mode is treated within the linear EV coupling approximation in the manner of Holstein[28] and is responsible for the formation of polaronic excitons.

We are now prepared to write down the aggregate Hamiltonian including site energy disorder and EV coupling involving the effective high-frequency intramolecular vibration with frequency, $\omega_0 = 1400\ cm^{-1}$. Written in a representation of one-excitons, $H$ reads:[15]

$$H = \omega_0 \sum_n b_n^\dagger b_n + \omega_0 \lambda \sum_n (b_n^\dagger + b_n)\, |n><n| + \sum_m \sum_n (J_{mn} + \Delta_m \delta_{mn})\, |m><n| + D + \omega_{0-0} + \lambda^2 \omega_0 \quad (1)$$

where $\hbar = 1$ is taken. The first term represents the vibrational energy due to the high-frequency mode, whereas the second term represents the linear EV coupling involving the same mode. $b_n^\dagger$ ($b_n$) is the creation (destruction) operator for vibrational quanta within the harmonic ground state nuclear potential on molecule $n$. The pure electronic state, $|n>$, indicates that the molecule at $n$ is electronically excited to the first optically allowed state, whereas all other molecules remain in their electronic ground states. The Huang−Rhys (HR) factor $\lambda^2$ measures the shift in the equilibrium positions of the ground and excited-state nuclear potentials. In what follows, we utilize an HR factor of $\lambda^2 = 1.2$, a value which, in conjunction with the cubic frequency dependence in the emission rate, yields roughly equal single molecule 0−0 and 0−1 emission peak intensities, as is found for OPV4 molecules in solution.[29] The excitonic coupling is mediated by $J_{mn}$ contained in the double summation term in eq 1. This term also contains the configuration-dependent transition frequency offset for the $n$th molecule, $\Delta_n$, relative to $\omega_{0-0}+D$, where $\omega_{0-0}$ is the gas-phase 0−0 transition frequency and $D$ is the gas-to-crystal shift induced by aggregation. Finally, in all that follows we utilize open boundary conditions. $H$ in eq 1 is referred to here on as the disordered Holstein (DH) Hamiltonian.

In this work, we utilize the two-particle approximation in representing eigenstates of the DH Hamiltonian. The αth excitonic wave function is therefore expanded as[30]

$$|\psi^{(\alpha)}> = \sum_{n,\tilde{v}} c_{n,\tilde{v}}^{(\alpha)} |n,\tilde{v}> + \sum_{n,\tilde{v}} \sum_{n',v'} c_{n,\tilde{v};n'v'}^{(\alpha)} |n,\tilde{v};n',v'> \quad (2)$$

The first term in eq 2 represents a delocalized vibronic excitation. The state $|n,\tilde{v}>$ consists of a vibronically excited chromophore at site $n$ with $\tilde{v}$ excited-state quanta in the (shifted) excited-state nuclear potential (see Figure 2). Because all other molecules are electronically and vibrationally unexcited, the state $|n,\tilde{v}>$ is also referred to as a single-particle state. The second term in eq 2 represents a delocalized vibronic/vibrational *pair* excitation. In addition to the vibronic excitation at $n$, the two-particle state, $|n,\tilde{v};n',v'>$, includes a vibrational excitation at $n'$ with $v'$ quanta in the ground state potential as demonstrated

(23) Mayo, S. L.; Olafson, B. D.; Goddard, W. A. *J. Phys. Chem.* **1990**, *94*, 8897−8909.
(24) Schreiber, M.; Toyozawa, Y. *J. Phys. Soc. Jpn.* **1982**, *51*, 1528−1536.
(25) Knapp, E. W. *Chem. Phys.* **1984**, *85*, 73−82.
(26) Gierschner, J.; Mack, H.-G.; Luer, L.; Oelkrug, D. *J. Chem. Phys.* **2002**, *116*, 8596−8609.
(27) Narwark, O.; Meskers, S. C. J.; Peetz, R.; Thorn-Csanyi, E.; Bässler, H. *Chem. Phys.* **2003**, *294*, 1−15.
(28) Holstein, T. *Ann. Phys.* **1959**, *8*, 325−342.
(29) Cornil, J.; Beljonne, D.; Heller, C. M.; Campbell, I. H.; Laurich, B. K.; Smith, D. L.; Bradley, D. D. C.; Müllen, K.; Brédas, J. L. *Chem. Phys. Lett.* **1997**, *278*, 139−145.
(30) Spano, F. C. *J. Chem. Phys.* **2002**, *116*, 5877−5891.

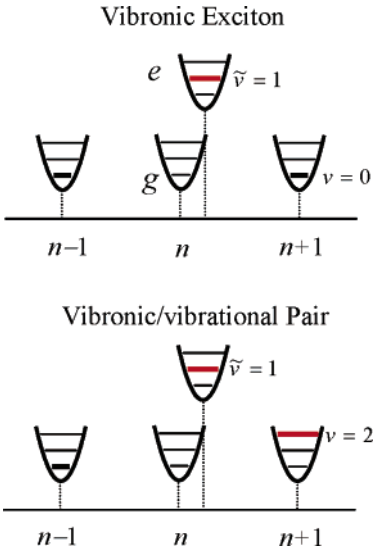


***Figure 2.*** Examples of the fundamental excitations in ordered organic assemblies. The vibronic (single-particle) excitation is $|n,\tilde{v} = 1>$ while the vibronic/vibrational pair (two-particle state) is $|n,\tilde{v} = 1; n + 1,v = 2>$.

schematically in Figure 2. One can also include three- and higher particle states; however, truncating at the two-particle level as in eq 2 is highly accurate in the intermediate coupling regime appropriate to MOPV4 helices, where the vibrational energy, $\omega_0$, the vibronic relaxation energy, $\lambda^2\omega_0$, and the (free) exciton bandwidth, $W$, are all comparable in magnitude.[30] The *free* exciton bandwidth, $W$, is the spectral separation between the highest and lowest energy excitons in the absence of disorder and exciton-vibrational coupling. For example, in a long linear aggregate with nearest-neighbor coupling ($J_0$) only, $W = 4J_0$. In the present case, where extended interactions are retained, $W$ is evaluated numerically from the DH Hamiltonian after setting $\Delta_n$, $\lambda^2$, and $\omega_0$ to zero.

In all calculations to follow, we also invoke an effective single-strand approximation (SSA), which assumes that the transition energies of the two molecules in an H-bonded pair (dimer) are identical, although the transition energy of each dimer may vary along the strand. Because the molecular transition dipole moments in the dimer are aligned only the in-phase electronic excitation on dimer $n$,

$$|n^+> \equiv \frac{1}{\sqrt{2}}\{|n_A> + |n_B>\}$$

is optically allowed, where $n_A$ and $n_B$ refer to local electronic excited states on molecules $A_n$ and $B_n$ (corresponding to strands $A$ and $B$, respectively, see Figure 1) within the $n$th dimer. The out-of-phase combinations along the strand are optically dark and do not couple to the in-phase states. They are therefore neglected. Hence, under the SSA, each H-bonded dimer can be treated as a single chromophore, thereby doubling the maximum aggregate length that can be analyzed numerically. The "effective" excitonic interaction between the chromophores at $n$ and $m$ is then, $<m^+|H|n^+> = J_{mn}$, with

$$J_{mn} \equiv J_{mn}^{AA} + J_{mn}^{AB} \tag{3}$$

$J_{mn}^{AA}$ ($J_{mn}^{AB}$) are the INDO/CCSD computed interactions between molecules $A_m$ and $A_n$ ($A_m$ and $B_n$). In deriving eq 3, we have also used $J_{mn}^{BB} = J_{mn}^{AA}$. A plot of $J_{mn}$ vs the inter-choromophore separation is shown in Figure 3 for several pitch angles.

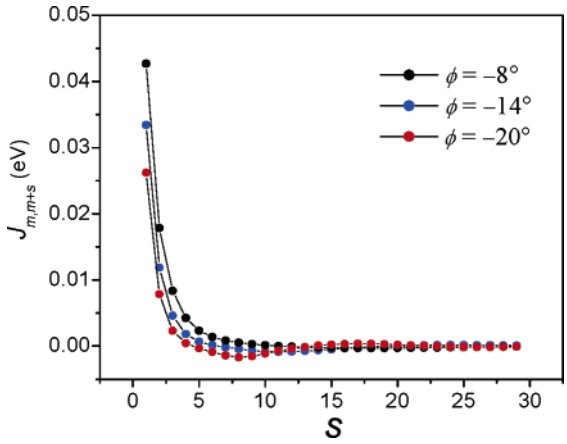


***Figure 3.*** Effective excitonic couplings, $J_{m,m+s}$ from eq 3 as a function of interchomophore distance, $s$, for several pitch angles.

The SSA treats the MOPV4 helix as an effective *single* strand of $N$ chromophoric units with interactions $J_{mn}$ from eq 3 between local excited states $|m>$ and $|n>$ (dropping the symmetry notation). Eigenstates and energies are computed from the Hamiltonian in eq 1 in a representation of eq 2 using the molecular parameters ($\omega_0$, $\lambda^2$) as discussed previously for each chromophoric unit. The SSA becomes exact as the interactions between molecules in strands $A$ and $B$, which are relatively weak in MOPV4 helices, approach zero. For MOPV4, we have confirmed the validity of the SSA by calculating the absorption and emission spectrum for a complete aggregate consisting of 10 H-bonded dimers ($N = 20$ molecules) and for and effective aggregate of $N = 10$ chromophoric units, in both cases without disorder. The spectra were in excellent agreement and virtually super-imposable.

Disorder can have a strong influence on the photophysical behavior of molecular aggregates. It may be taken into account by assuming a statistical distribution for the values of the interchormophoric couplings ($J_{mn}$, off-diagonal disorder) and for the site energies (diagonal disorder). Although off-diagonal disorder may be important,[31] we neglect it here for the sake of simplicity and consider only diagonal disorder. We assume that the site energies for the chromophores in the effective single strand are distributed randomly, but with spatial correlation. Following Knapp,[25] we assume a joint Gaussian distribution of transition frequency offsets:

$$P(\Delta_1,...,\Delta_N) = \frac{1}{(2\pi)^{N/2}\sqrt{\det A}} \exp\left(-\sum_{n,m=1}^{N} \frac{1}{2}(A^{-1})_{m,n}\Delta_n\Delta_m\right) \tag{4}$$

where $(A^{-1})_{m,n}$ is the $mn$th element of the inverse covariance matrix.[32] In linear aggregates with open boundary conditions, elements of the covariance matrix are given by

(31) Jang, S.; Dempster, S. E.; Silbey, R. J. *J. Phys. Chem. B.* **2001**, *105*, 6655–6665.

(32) Equation 4 contains factors of 2 which were inadvertently omitted from the distribution function reported in ref 15, although the correct distribution as shown in eq 4 was used throughout.

$$A_{nm} \equiv <\Delta_n \Delta_m>_C = \frac{\sigma^2}{2} \exp(-|n-m|/l_0) \qquad (5)$$

Here, $<...>_C$ denotes a configurational average over random transition-offset distributions and $\sigma$ measures the magnitude of the disorder, through the single-site variance $\sigma^2/2 = <\Delta_n^2>_C$. Note that our definition of $\sigma$ is $\sqrt{2}$ times that used by Knapp.[25] In eq 5, $l_0$ is the spatial correlation length in dimensionless units of lattice spacing. Alternatively, one can introduce the correlation parameter, $\beta \equiv \exp(-1/l_0)$, which ranges from zero when $l_0 = 0$ (no spatial correlation) to unity as $l_0$ approaches infinity. In the former case ($\beta = 0$), the distribution (eq 4) reduces to that used by Schreiber and Toyozawa,[24]

$$P(\Delta_1,...,\Delta_N) = \prod_{n=1}^{N} \frac{\exp(-\Delta_n^2/\sigma^2)}{\sqrt{\pi}\sigma} \qquad (6)$$

and the transition frequency offsets for each chromophore are chosen independently from a Gaussian distribution of (1/*e*) full-width, $2\sigma$. As $\beta$ approaches unity all chromophores within a given aggregate have identical offsets, the values of which are distributed over the aggregate ensemble according to a normal distribution (1/*e* width of $2\sigma$). The distribution (eq 4) has recently been used to successfully account for the emission line shape in *poly*(3-hexylthiophene) in ref 15.

Once the excitonic wave functions, $|\psi^{(\alpha)}>$ , and transition frequencies, $\omega_{\alpha,}$ for a given configuration of offsets have been evaluated numerically the absorption, $A(\omega)$; emission, $S(\omega)$; absorption dissymmetry, $g_{abs}(\omega)$; and luminescence dissymmetry, $g_{lum}(\omega)$,[7] are readily evaluated by taking appropriate configurational and thermal averages. Full expressions for all spectral observables appear in the Supporting Information.

### III. Absorption and Emission Spectra

Before considering the four spectral observables separately, we present in Figure 4 an overview of the measured and theoretical spectra. For the latter, the only adjustable parameters are the pitch angle $\phi$ defining the helicity and the distribution parameters, $\sigma$ and $l_0$. To obtain optimal agreement with experiment, $\phi$ and $\sigma$ were varied to reproduce the absorption peak position and width, respectively. Subsequent analysis of the emission spectrum yielded $l_0$. Best fit values used in the Figure are $\phi = -14°$, $\sigma = 0.12$ eV and $l_0 = 4.5$ ($\beta = 0.8$). Here, the sign of $\phi$ is defined with respect to a left-handed helix in keeping to the convention of ref 18. The negative value therefore indicates a twist of $|\phi|$ in the right-hand helix as in Figure 1. All four calculated spectra utilize the same ($\sigma$, $l_0$) and $\phi$. For a given $\phi$, the choice of ($\sigma$, $l_0$) is unique; no other combination can simultaneously reproduce all four spectra with the same accuracy.

The theoretical spectra in Figure 4 are based on aggregates containing $N = 20$ chromophores (H-bonded dimers); $10^4$ configurations of transition energy offsets, [$\Delta_1$, $\Delta_2$,..., $\Delta_N$], were randomly generated according to the correlated distribution in eq 4. Eigenstates and energies of the DH Hamiltonian in eq 1 were obtained numerically for each configuration using the SSA and TPA approximations and subsequently inserted into the spectral averages in eqs S1−S4 (see Supporting Information). The discrepancies in the experimental/theoretical agreement in Figure 4, such as the small relative shift in $S(\omega)$ and the slight mismatch in the magnitudes of $g_{abs}(\omega)$ and $g_{lum}(\omega)$, can readily be accounted for as described below.

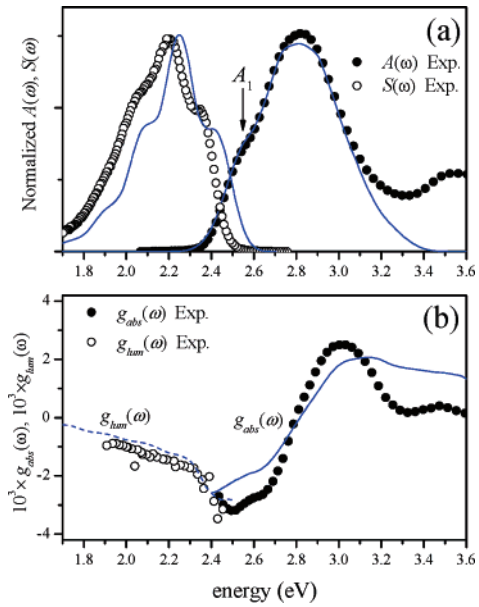


***Figure 4.*** (a) Experimental absorption, $A(\omega)$, and emission, $S(\omega)$, spectra of MOPV4 helices ([MOPV4] = $2 \times 10^{-5}$ M) at 278 K with (b) corresponding degrees of circular polarization in absorption $g_{abs}$ and luminescence $g_{lum}$. Also shown are the theoretical spectra (solid and dashed curves) based on the disordered Holstein Hamiltonian (see text).

**Absorption.** Figure 4a,b shows the measured absorption spectrum, $A(\omega)$, using unpolarized light, along with the degree of circular polarization in absorption, $g_{abs}(\omega)$ ($= 2(A_L - A_R)/(A_L + A_R)$ with $A_{L(R)}$ being the absorbance for left (right) circular polarized light). The absorption spectrum is rather broad but with a pronounced shoulder labeled $A_1$ at approximately 2.6 eV. $g_{abs}(\omega)$ has the classic bisignate form characteristic of delocalized excitations. Agreement between theory and experiment with regard to the sign of $g_{abs}(\omega)$ confirms the predominance of right-hand helices. Experiments have shown that the absorption shoulder as well as the entire dissymmetry spectrum grows in as the temperature is lowered to induce aggregation.[1,2]

Figure 5 shows the calculated $A(\omega)$ and $g_{abs}(\omega)$ for various spatial correlation lengths, $l_0$. Although our calculations employ the more sophisticated two-particle approximation, the single particle approximation (SPA) which utilizes only the first (vibronic) term in eq 2 yields essentially the same spectra as in Figure 5. This arises because $\sigma/W$ is sufficiently large (and the spectra sufficiently broad) to obscure two-particle effects.[33] Moreover, the vibronic/vibrational pair states (see Figure 2) carry no oscillator strength from the vibrationless ground state. Using the SPA we have confirmed that *both* $A(\omega)$ *and* $g_{abs}(\omega)$ remain essentially unchanged as $N$ increases beyond 20. Hence, the spectra in Figure 5 correspond as well to infinitely large aggregates.

The calculated spectra in Figure 5a very weakly depend on $l_0$; all are in excellent agreement with experiment up to ~3.1 eV, fully capturing the relative intensity and peak position of the $A_1$ shoulder. The disagreement in the higher energy region is due to additional excited states not included in the theory. The weak $l_0$ dependence arises because $\sigma$ is of the order of $W$ (= 0.15 eV) placing MOPV*n* aggregates well beyond the

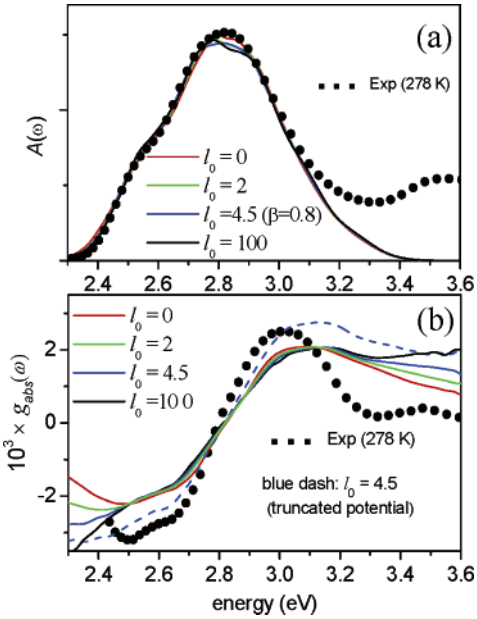


***Figure 5.*** Experimental absorption (a) and absorption dissymmetry (b) vs energy at $T = 278$ K (black dots). Also shown are the calculated spectra for $N = 20$ aggregates and several spatial correlation lengths. The free exciton bandwidth is 0.15 eV, slightly larger than the disorder width $\sigma = 0.12$ eV. The dashed curve in (b) corresponds to the truncated excitonic potential (see text).

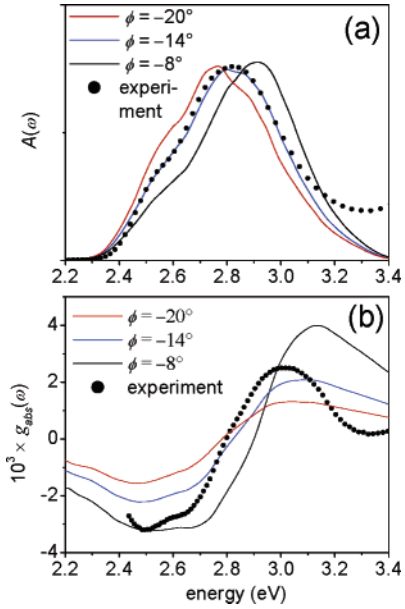


***Figure 6.*** Calculated absorption (a) and absorption dissymmetry (b) vs energy for $N = 20$ aggregates and for several values of aggregate pitch angle, $\phi$. In addition, $l_0 = \beta = 0$ and $\sigma = 0.12$ eV. Also shown are the experimental data at $T = 278$ K.

motional narrowing regime, where the absorption spectral width narrows with decreasing $l_0$.[25]

The structure of the absorption spectrum is characteristic of strong exciton−phonon coupling in linear aggregates.[15] Here, excited states are grouped into vibronic bands, starting with the lowest $\tilde{v} = 0$ band comprised mainly of single-particle states, $|n,\tilde{v} = 0>$, whose delocalization is controlled by the ratio of the disorder width, $\sigma$, to the $\tilde{v} = 0$ vibronic bandwidth, $W \exp(-\lambda^2)$. The $A_1$ shoulder arises from such states and correlates to the 0−0 transition in the single molecule spectrum when the excitonic couplings vanish. It was previously shown that the intensity of $A_1$ relative to the main absorption peak diminishes with increasing exciton bandwidth,[15,33] making the relative $A_1$ peak intensity a useful measure of the electronic coupling. This was strictly shown for the case of achiral aggregates but remains valid for chiral aggregates as well, as we will show in greater detail in a future publication. The bisignate form of $g_{abs}$ in Figure 5b also reflects excitonic coupling and provides an additional check on the exciton bandwidth.

The sensitivity of the absorption spectra to the pitch angle, $\phi$, is shown in Figure 6. Increasing the pitch angle decreases the overlap between neighboring molecules and hence reduces the exciton bandwidth, $W$. We find that for $\phi = -8, -14$, and $-20°$, the respective values of $W$ are 0.21, 0.15, and 0.11 eV. Hence, the $\phi = -8°$ spectrum is shifted furthest to the blue, with the smallest $A_1$ shoulder intensity, whereas the opposite is true for $\phi = -20°$.

The calculated absorption spectra in Figures 5a and 6a were normalized so that the peak height coincides with experiment. This can be rationalized as a fitting procedure for the magnitude of the transition dipole moment or optical path length. However, this is not possible for $g_{abs}$ ($\omega$), which is an intensive quantity *independent* of the transition dipole moment and path length. By definition, $g_{abs}$ represents the net degree of circular polarization normalized to the total absorption (see Supporting Information). Figures 4b and 5b show that the calculated $g_{abs}$ ($\omega$) reproduces the experimental line shape but is reduced in magnitude by about 30%. Consistent with earlier analysis,[14] $g_{abs}$ ($\omega$) is far more sensitive to extended interactions than absorption. A strong possibility for the 30% disparity is an overestimation of the extended excitonic interactions $J_{mn}$ due to our neglect of dielectric screening effects. To demonstrate this we have recalculated $g_{abs}$ after truncating the excitonic couplings beyond the *sixth* nearest neighbor; i.e. $J_{m,\ m+s}$ was set to zero for $s > 6$. The truncation has a negligible effect on the absorption spectrum, producing a minute red-shift of less than 0.005 eV, almost imperceptible on the scale of Figure 5a. By comparison, the change in $g_{abs}$ is far greater. The dashed curve in Figure 5b shows $g_{abs}(\omega)$ for the truncated potential. The increase in $|g_{abs}|$ in the $A_1$ region is quite substantial and results in a vastly improved agreement with experiment.

**Emission.** As depicted in Figure 4a, in contrast to absorption the vibronic progression is more clearly resolved in emission, making it tempting to describe emission using a smaller disorder width, $\sigma$. Aggregation effects in emission include a reduction in the relative 0−0 peak intensity (compared to the 0−1 intensity) by about a factor of 2 compared to the single molecule in solution obtained at higher temperatures.[1] Moreover, the polarization dissymmetry is entirely aggregation-induced; the measured $g_{lum}(\omega)$ becomes negligibly small in hydrogen bonding solvents in which MOPV4 does not form aggregates (See Supporting Information). The measured $|g_{lum}|$ (Figure 4b) gradually increases with energy through the sideband transitions, with a far more rapid rise in the vicinity of the highest-energy 0−0 transition. Such behavior is characteristic of other small

(33) Spano, F. C. *Chem. Phys.* **2006**, *325*, 22−35.

molecular and polymeric organic systems.[34−36] In what follows, we show that all of the aforementioned properties are consistent with vibrationally dressed excitons extending over several molecules.

The numerically calculated emission observables for several $l_0$ are shown in Figures 7 and 8. The disorder width, $\sigma = 0.12$ eV, is *identical* to that used in modeling absorption in Figures 4 and 5. The calculated emission is comprised of a superposition of emission from all aggregates in the ensemble, *and* from a Boltzmann distribution of emitting states within $4kT$ of the exciton band bottom for each aggregate, with $T = 278$ K taken to coincide with experiment. (We verified that states beyond $4kT$ of the band bottom contribute negligibly to emission.) The emitting distribution assumes rapid intraband relaxation on a time scale shorter than the emission lifetime.

In contrast to absorption, which is determined almost entirely from the vibronic exciton component of the various excited states, emission also contains significant contributions from the vibronic/vibrational pair states. In refs 37 and 38 it was shown that one- and two-particle interferences lead to profound reductions in the sideband emission intensities, consistent with aggregation-induced fluorescence quenching. In the present example ($\sigma = 0.12$ eV, $l_0 = 4.5$), our calculations show an increase by about a factor of 2 in the 0−1 peak intensity when the vibronic/vibrational states in eq 2 are omitted-i.e. under the SPA. (We note that the 0−0 peak is unique in that it depends, as does absorption, only on single-particle coefficients.) The CPL dissymmetry presents a more dramatic example of the importance of the vibronic/vibrational pair states. Here, the dissymmetry, $g_{lum}$, of the emission side-bands is rigorously zero if only single-particle coefficients are retained.[18] Thus, $g_{lum}$ directly probes the extent of the nuclear distortion field, as we show in greater detail below.

Let us first consider the emission spectrum, $S(\omega)$. One of the more remarkable features in Figure 7 is the relative reduction of the 0−0 intensity peak with increasing spatial correlation. This is clearly seen in the spectra of Figure 7b, which are normalized to the peak intensities, and is quantified by the ratio of the 0−0 to 0−1 peak intensities,

$$S_R \equiv \frac{S(\omega = \omega^{0-0})}{S(\omega = \omega^{0-1})} \tag{7}$$

For an isolated chromophore, $S_R$ reduces to $S_R = (\lambda^2 f_1^3)^{-1}$ using FC factors for displaced harmonic oscillators. Here, $f_1$ is the 0−1 emission frequency normalized by the 0−0 emission frequency. When $\lambda^2 = 1.2$ and $f_1^3 \approx 0.8$, as is appropriate for OPV4 chromophores, $S_R$ takes the value of 1.04. By contrast, the measured and theoretical values of $S_R$ from Figure 7 are substantially smaller than unity, with the experimental value approximately 0.65. This discrepancy is due entirely to the effects of aggregation, as we show below.

Figure 7b shows how $S_R$ diminishes with increasing spatial correlation at $T = 278$ K. A far more dramatic demise with $l_0$ occurs at lower temperatures as indicated in Table 1. Table 1 also shows that $S_R$ diminishes with decreasing $\sigma$ and/or increasing $l_0$ becoming essentially zero for homogeneous aggregates ($\sigma \rightarrow 0$ or $l_0 \rightarrow \infty$) at low temperature. In general, the relative 0−0 intensity increases with increasing *intra-aggregate* disorder and also with increasing temperature (dynamic disorder).

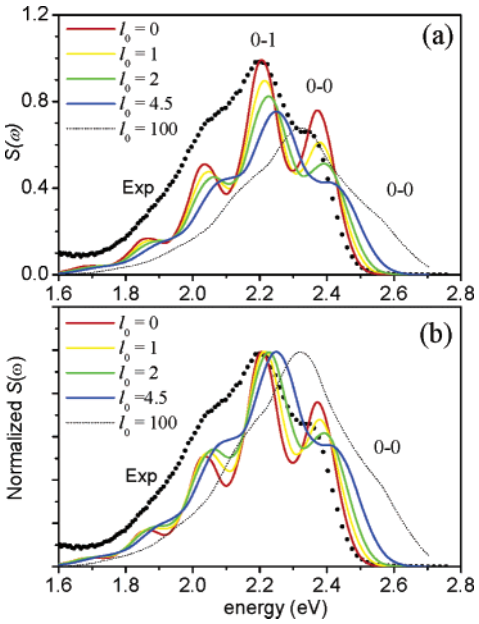


***Figure 7.*** Calculated PL spectra vs energy for $N = 20$ helices with $\phi = -14°$ and for several values of the spatial correlation, $l_0$. Also shown is the experimental data at $T = 278$ K. In (b), spectra are normalized to the 0−1 peak intensity.

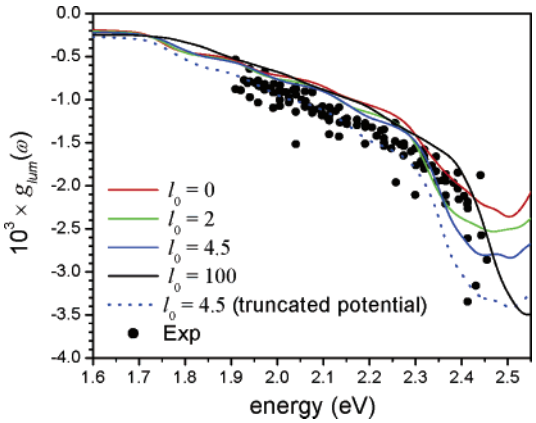


***Figure 8.*** Experimental CPL dissymmetry as a function of photon energy at $T = 278$ K (solid dots). Also shown are the calculated dissymmetry spectra for $N = 20$ helices with $\phi = -14°$ and $\sigma = 0.12$ eV and for several spatial correlation lengths. The dashed curve corresponds to the truncated excitonic potential (see text).

Although the results in the Table applied to aggregates with $N = 20$ chromophores, our calculations show that $S_R$ is practically constant from $N = 4$ to 20. We conclude that $S_R$ remains a useful measure of ($\sigma$, $l_0$) independent of $N$.

The strong dependence of $S_R$ on ($\sigma$, $l_0$) reflects the coherent nature of the emitting exciton(s). For achiral aggregates ($\phi = 0$) without any static or dynamic disorder ($\sigma = 0$, $T = 0$ K)—so that the emitting exciton is delocalized over the *whole* aggregate—the 0−0 peak (and therefore $S_R$) vanishes rigorously due to symmetry.[13,14] This is the case of an ideal H-aggregate where the exciton wavefunction at the bottom of the band is odd with

(34) Meskers, S. C. J.; Peeters, E.; Langeveld-Voss, B. M. W.; Janssen, R. A. J. *Adv. Mat.* **2000**, *12*, 589−594.
(35) Langeveld-Voss, B. M. W.; Janssen, R. A. J.; Meijer, E. W. *J. Mol. Struct.* **2000**, *521*, 285−301.
(36) Langeveld-Voss, B. M. W.; Beljonne, D.; Shuai, Z.; Janssen, R. A. J.; Meskers, S. C. J.; Meijer, E. W.; Brédas, J. L. *Adv. Mater.* **1998**, *10*, 1343−1348.
(37) Spano, F. C. *J. Chem. Phys.* **2003**, *118*, 981−994.
(38) Spano, F. C. *J. Chem. Phys.* **2001**, *114*, 5376−5390.

***Table 1.*** Ratio of the Calculated 0−0 and 0−1 Vibronic Band Intensities in the Luminescence Spectrum of the MOPV4 Aggregate ($S_R$), as a Function of the Disorder Parameter ($\sigma$) and the Disorder Correlation Length ($l_0$)

| $l_0$ ($\beta$) | $\sigma$(eV) | $S_R$ at $T = 0$ K | $S_R$ at $T = 278$ K |
|---|---|---|---|
| 100 (0.99) | 0.12 | ∼0 | 0.40 |
| 4.5 (0.8) | 0.12 | 0.40 | 0.56 |
| 0 (0) | 0.12 | 0.65 | 0.75 |
| 4.5 (0.8) | 0.06 | 0.22 | 0.41 |
| 4.5 (0.8) | 0.012 | 0.014 | 0.41 |

respect to a reflection through the plane bisecting the aggregate. For aggregates with periodic boundary conditions the same conclusion is arrived at by appealing to the familiar $\Delta k = 0$ selection rule for optical transitions. The selection rule is violated in 0−0 emission since the bandbottom exciton has $k = \pi$ while the ground state carries no momentum. This contrasts the case for the replica (0−1, 0−2,...) transitions, which are able to maintain momentum conservation by terminating on electronic ground states with one or more phonons of the appropriate wave vector(s).[37] Hence, in ideal achiral H-aggregates with no disorder only sideband emission remains.

Introducing disorder in achiral H-aggregates breaks the symmetry and allows 0−0 emission. Hence, the 0−0 intensity increases with increasing $\sigma$ and/or decreasing $l_0$.[15,39] Interestingly, even in the presence of strong disorder ($\sigma \gg W$), $S_R$ can become small as long as the spatial correlation length, $l_0$, remains large. This is most dramatically demonstrated in the limit of maximum correlation ($\beta = 1$ or $l_0 = \infty$) where the coherence range once again covers the entire aggregate. In this so-called long-range inhomogeneous broadening limit, the 0−0 intensity vanishes, independent of the magnitude of $\sigma$.

Figure 7 and Table 1 show that a qualitatively similar dependence of $S_R$ on disorder exists for chiral aggregates. The lowest energy exciton in helical aggregates with periodic boundary conditions, an integral number of full turns and with no disorder is rigorously optically dark[14] so that no 0−0 emission can occur. Table 1 shows that the same is essentially true in helical aggregates with open boundary conditions and vanishing intra-aggregate disorder (see $T = 0$, and $l_0 = 100$ entry). As in the achiral case, increasing disorder breaks the symmetry, leading to increased 0−0 emission (and $S_R$). Because the exciton coherence range, denoted as $N_{coh}$, decreases with increasing intra-aggregate disorder, $S_R$ depends on $N_{coh}$ in an inverse manner; $S_R$ therefore provides a measure of $N_{coh}$ as well as the spatial correlation length $l_0$. Furthermore, the increase of $S_R$ with temperature can be viewed as an inverse dependence on the thermal coherence number.[40] When $kT \gg W$, $S_R$ tends to the single molecule value. Figure 7 shows that at $T = 278$ K, the value of $l_0$ which best agrees with experiment is approximately 2−4 molecules ($\beta = 0.6$−$0.8$).

In addition to the relative line intensities, the emission line widths and peak positions also depend on spatial correlation. As Figure 7 shows, the vibronic peaks broaden by approximately a factor of 2 and shift to the blue by ∼0.12 eV as the correlation length $l_0$ increases from 0 to 100. For large $l_0$ (>100), the full width at (1/$e$) tends toward $2\sigma = 0.24$ eV and the vibronic lines are barely resolvable. Because $\sigma$ is fixed from the absorption analysis ($\sigma = 0.12$ eV), the emission line width provides yet another check on the spatial correlation length $l_0$. In Figure 7, the line width agrees with experiment when $l_0 \approx 4.5$ ($\beta = 0.8$), consistent with our previous estimates based $S_R$. However, the calculated spectrum is slightly blue-shifted by ∼0.04 eV compared to the experimental spectrum.

The calculated line narrowing as $l_0$ approaches zero in Figure 7 is qualitatively similar to Knapp's enhancement of motional narrowing as spatial correlation vanishes,[25] but arises from a distinctly different physical mechanism because $\sigma/W$ is too large to support motional narrowing regime. Instead, the emission narrowing and red-shifting with decreasing $l_0$ are both due to the enhanced ability of excitons to find deep traps as site energies become uncorrelated, consistent with our assumption that emission is rapidly equilibrated to the exciton band-bottom. As we show in a follow-up publication the distribution of such low-energy traps is generally narrower than $2\sigma$. Because finding low-energy traps is more probable in larger aggregates, we also expect both the spectral narrowing and red-shifting to increase with $N$, and indeed, we have confirmed this numerically.

Let us now turn our attention to the final observable $g_{lum}$. The increase of $|g_{lum}(\omega)|$ with $\omega$, and especially the rapid rise in the vicinity of the emission origin, quantified here by the ratio

$$G_R \equiv \frac{g_{lum}(\omega = \omega^{0-0})}{g_{lum}(\omega = \omega^{0-1})} \tag{8}$$

was originally accounted for qualitatively in ref 18, where it was shown that the 0−0 dissymmetry behaves quite differently than the replicas. The situation is analogous to the unique linear polarization of the 0−0 emission found in herringbone aggregates of conjugated achiral oligomers[17,19,37] and underscores how aggregation affects the emission origin in a manner quite distinct from the replicas. For example, the 0−0 intensity is sourced entirely by the vibronic exciton portion of the emitting wave function (see eq 2), whereas replica intensities also contain significant vibronic/vibrational contributions. The uniqueness of the 0−0 dissymmetry is most pronounced in homogeneous ($\sigma = 0$) aggregates with weak excitonic coupling ($W \ll \lambda^2\omega_0$) at low temperature.[18] The dissymmetry is uniform over each narrow, well resolved vibronic peak, taking on the value

$$g_{lum}^{0-\nu_t} \equiv R_{lum}^{0-\nu_t}/I^{0-\nu_t} \tag{9}$$

for the $0-\nu^t$ peak, where $R_{lum}^{0-\nu_t}$ is the rotational strength and $I^{0-\nu_t}$ is the unpolarized emission line strength (see Supporting Information). Using the physically relevant parameter set for MOPV4 aggregates ($\lambda^2 = 1.2$, $\phi = -14°$, and $W = \omega_0$) gives $G_R = g_{lum}^{0-0}/g_{lum}^{0-1} \approx -200$ for an homogeneous aggregate with $N = 20$ molecules. The experimental enhancement observed in Figure 8 is 2 orders of magnitude smaller and of opposite sign. However, when disorder, nonzero $T$, and extended interactions are fully incorporated, the calculated dissymmetry, as displayed in Figure 7, reproduces the experimental line shape quite well, capturing the steady increase of $|g_{lum}(\omega)|$ with $\omega$ as well as the modest surge ($G_R \approx 2$) in the vicinity of the 0−0 emission. The reduction of $|G_R|$ from the disorder-free value is primarily a result of increased localization of the emitting exciton as we will show in a future publication.

(39) Meskers, S. C. J.; Janssen, R. A. J.; Haverkort, J. E. M.; Wolter, J. H. *Chem. Phys.* **2000**, *260*, 415−439.
(40) Spano, F. C. *J. Chem. Phys.* **2004**, *120*, 7643−7658.

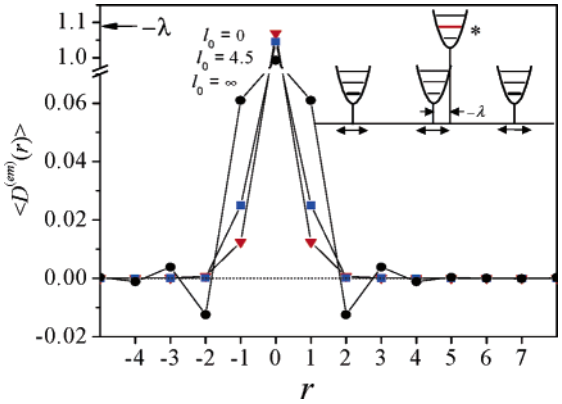


***Figure 9.*** Nuclear distortion field calculated for the emitting exciton in a MOPV4 helix containing $N = 20$ chromophore units with $\lambda = -(1.2)^{1/2}$, $\phi = -14°$ and $\sigma = 0.12$ eV. Three spatial correlation lengths are shown, $l_0$=0 (red triangles), $l_0$=4.5 (blue squares) and $l_0$=∞ (black circles).

The magnitude of the calculated $|g_{lum}(\omega)|$ also agrees well with experiment, and is only about 20−30% smaller than the measured values over the entire spectral range. As was the case for $g_{abs}(\omega)$, we attribute the slight disparity to the neglect of dielectric screening. To test our idea, we also show in Figure 8 $g_{lum}(\omega)$ corresponding to the truncated excitonic potential in which all interactions $J_{m,\ m+s}$ for $s > 6$ are set to zero. As in the case of $g_{abs}(\omega)$, the magnitude of the response increases to the point where $g_{lum}(\omega)$ is in excellent agreement with experiment. Although not shown, the effect of truncation on $S(\omega)$ is negligible by comparison. In a future paper we will present a detailed account of the polarization dissymmetry including an expression for the dependence on extended interactions.

Figure 8 further shows that $g_{lum}$ is mainly sensitive to spatial correlation only in the 0−0 spectral region, with the value $l_0$= 4−5 reproducing the value ($G_R \approx 2$) observed in experiment. $G_R$ like $S_R$ is therefore a useful measure of spatial correlation. This property can be traced back to the homogeneous limit, where the replica dissymmetries, $g_{lum}^{0-\upsilon_t}$ ($\upsilon_t \geq 1$), are independent of size, $N$, in marked contrast to $g_{lum}^{0-0}$. The decrease in $G_R$ with disorder is associated with a reduction of the coherence range of the exciton. In the next Section, we determine the extent of this localization.

## IV. Excited State Characterization

On the basis of the excellent agreement obtained for the four photophysical observables in the previous section, we can now describe with some confidence the nature of the (neutral) optical excitations in MOPV4 helices. In this section, such excitations are characterized in two ways: (i) the spatial extent of the nuclear distortion field-or phonon cloud-surrounding the electronic excitation, and (ii) the coherence range of the composite exciton, which can also be referred to as a neutral polaron.

The nuclear displacement field corresponding to the αth excited state, $\psi^{(\alpha)}$, is,[37]

$$D^{(\alpha)}(r) \equiv \langle\psi^{(\alpha)}|\{\sum_n |n\rangle\langle n|b_{n+r}\}|\psi^{(\alpha)}\rangle \qquad (10)$$

and measures the dimensionless deviation of the vibrational coordinate (relative to the ground state minimum) in a chromophore $r$ lattice spacings from the vibronically excited chromophore—see Figure 9. In an isolated molecule, for example, the deviation is $D^{(\alpha)}(0) = -\lambda$ for all vibronic

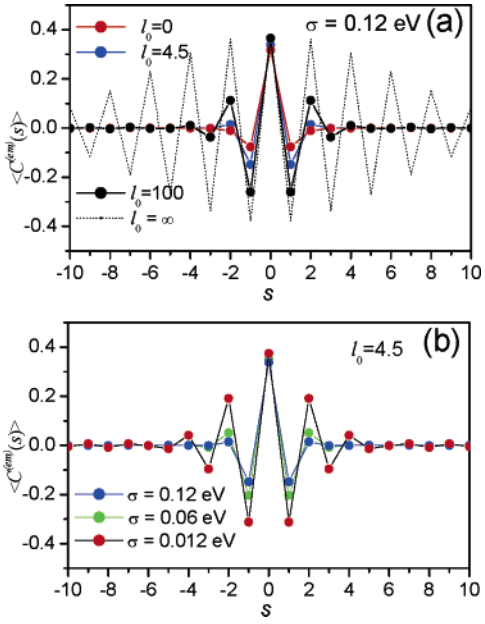


***Figure 10.*** Exciton coherence function for the emitting exciton in an aggregate containing 20 molecules. In (a), $\sigma = 0.12$ eV is held constant as $l_0$ is varied, whereas in (b), $l_0 = 4.5$ ($\beta = 0.8$) is held constant whereas $\sigma$ is varied.

excitations because all excited eigenstates (with zero, one,... quanta) are centered about the shifted nuclear potential by $-\lambda$. (A negative value for $\lambda$ corresponds to an *increase* in the nuclear coordinate relative to the minimum in the ground state potential). The shift in the nuclear coordinate in proper units of distance is determined from $\Delta R = -\lambda\sqrt{2\hbar\omega_0/k_p}$, where $k_p$ is the curvature of the harmonic potential.

For an H-aggregate in the weak to intermediate excitonic coupling regime, the low-energy polarons are characterized by $|D^{(\alpha)}(0)| \tilde{<} |\lambda|$, i.e., the centrally excited chromophore is almost fully shifted, but neighboring molecules, although not electronically excited, are nevertheless displaced along the nuclear coordinate to a degree which decreases with $|r|$.[37]

Figure 9 shows the spatial dependence of the distortion field for the emitting exciton in MOPV4 aggregates averaged over 1000 configurations of site disorder using $\lambda = -\sqrt{1.2}$ and varying degrees of spatial correlation. The Figure shows that the vibronically excited chromophore ($r = 0$) undergoes a shift in its geometry which is almost as large as in an isolated, excited MOPV molecule. In the aggregate, the nuclear distortion spreads out so that the neighboring molecules with $|r| = 1$ undergo small displacements, even though they formally do not carry the electronic excitation at the moment under evaluation. The distortions at $|r| = 1$ reflect the contribution of the vibronic/vibrational pairs states to the exciton (see Figure 2) and in a time dependent picture, these distortions result from the presence of the excitation at the neighbor molecules with $|r| = 1$ a few moments earlier. This illustrates the inseparability of the nuclear and electronic motion. The distortion of the neighbor molecules with $|r| = 2$ are even smaller than for $|r| = 1$. Curiously, when $l = \infty$, the small distortion for $|r| = 2$ is in a direction opposite to that of the isolated excited molecule, indicating a very intricate dynamical behavior of the exciton that needs to be analyzed further.

When $l_0 = 4.5$, the spatial correlation that best describes MOPV4 aggregates, the extent of the nuclear distortion sur-

rounding the vibronically excited molecule, is limited to nearest neighbors where the nuclear displacement is approximately 2.5% of the total single molecule vibronic shift ($|\lambda|$). The shift is due to the vibronic/vibrational pair states present in the emitting wave function (see eq 2)—when $|r| \geq 1$, the displacement is dominated by the leading term

$$D^{(\mathrm{em})}(r) \approx \sum_{n,\tilde{\nu}} c^{(\mathrm{em})}_{n\tilde{\nu}} c^{(\mathrm{em})}_{n\tilde{\nu};n+r,\upsilon=1}\bullet \quad |r| \geq 1 \tag{11}$$

The very same two-particle coefficients in eq 11 give rise to the sideband polarization dissymmetry, $g_{lum,}$ as shown in ref 18 (see eq 14b there). Hence, analysis of $g_{lum}(\omega)$ using the Hamiltonian in eq 1 allows one to identify the vibronic/vibrational component of the emitting exciton. We can of course analyze all of the excitons in a similar manner.

We next determine the coherent range $N_{\mathrm{coh}}$ of the emitting exciton (polaron) − in other words the number of molecules over which the center-of-mass of the neutral polaron is coherently delocalized. To quantify $N_{\mathrm{coh}}$, we first introduce the exciton coherence function for the αth exciton as

$$C^{(\alpha)}(s) \equiv \sum_{n} < \psi^{(\alpha)}|B_n^+ B_{n+s}|\psi^{(\alpha)} > \tag{12}$$

where $B_n^+$ is the local exciton creation operator, given by $B_n^+ \equiv |n;\upsilon ac >< g;\upsilon ac|$. Here, $|n;\upsilon ac >$ represents the vibronic state with molecule $n$ excited electronically with all molecular vibrations (on all sites) remaining in the vacuum state. $|g;\upsilon ac >$ is the electronic/vibrational ground state. Inserting the exciton wave function (eq 2) into the coherence function (eq 12) gives

$$C^{(\alpha)}(s) = \sum_{n} \sum_{\tilde{\nu},\tilde{\nu}'} c^{(\alpha)}_{n\tilde{\nu}}\, c^{(\alpha)}_{n+s\tilde{\nu}'}\, f_{\tilde{\nu}0} f_{\tilde{\nu}'0} \tag{13}$$

where $f_{\tilde{\nu}\nu'} \equiv <\tilde{\nu}|\nu'>$ is the vibrational overlap factor between the vibrational state with $\tilde{\nu}$ quanta in the shifted, excited-state potential and the vibrational state with $\nu'$ quanta in the ground electronic potential. Equation 13 shows that $C^{(\alpha)}(s)$, like the 0−0 emission intensity, is solely a function of single particle coefficients. In fact, using eqs S6 (see Supporting Information) and 13 shows the 0−0 intensity to be simply related to the correlation function through, $I^{0-0} = \sum_s C^{(\mathrm{em})}(s)\cos(\phi s)$.

Figure 10a shows the coherence function as a function of separation $s$ for the lowest energy (emitting) exciton in a chiral ($\phi = -14°$) aggregate with $\sigma = 0.12$ eV and for several values of $l_0$. The coherence function is averaged over several thousand disorder configurations. The phase oscillations are characteristic of a band bottom exciton in an ideal H-aggregate ($\phi = 0$), which is expected because $|\phi|$ is small. In the limit $l_0 = \infty$, the absence of *intra*-aggregate disorder leads to an extended $k = \pi$ exciton when periodic boundary conditions are invoked. However, all calculations reported here utilize open boundary conditions. In this case, the coherence range for $l_0 = \infty$ extends over the entire aggregate as shown in Figure 10 but diminishes with $|s|$ due to end effects—similar to the wave functions in the particle-in-a-box.

Figure 10a shows how the coherence size $N_{\mathrm{coh}}$ of the emitting exciton increases with spatial correlation while remaining substantially smaller than $l_0$. $N_{\mathrm{coh}}$ is taken to be $1 + s_{max}$, with $s_{max}$, the maximum $|s|$ for which

$$|< C^{(\mathrm{em})}(s) >_c| \;>\; 0.01\,|< C^{(\mathrm{em})}(0) >_c| \tag{14}$$

With this definition, $N_{\mathrm{coh}}$ tends to unity in the limit of complete localization, where $<C^{(\mathrm{em})}(s)>_c$ becomes nonzero only at $s = 0$. Figure 10a shows that when $l_0 = 100$, $N_{\mathrm{coh}}$ is only 5. This disparity between $l_0$ and $N_{\mathrm{coh}}$ arises because $N_{\mathrm{coh}}$ depends on *both* $\sigma$ and $l_0$. In the extreme example of very strong disorder, (not shown) complete localization ($N_{\mathrm{coh}} = 1$) obtains for *any* $l_0$ as $\sigma/W$ approaches infinity. The value of $\sigma$ used in Figure 10a is slightly less than the exciton bandwidth, $W$, but large enough to make $N_{\mathrm{coh}}$ significantly less than $l_0$. The effect of increasing $\sigma$ while holding $l_0$ constant is demonstrated in Figure 10b, which shows $N_{\mathrm{coh}}$ diminishing with $\sigma$. In conclusion, low-energy excitons are coherently localized with $N_{\mathrm{coh}} < l_0$, with the exact value of the coherence size depending on $\sigma/W$. In the case of MOPV4 aggregates with $l_0 = 4.5$ ($\beta = 0.8$), Figure 10a predicts a coherence range of only 2−3.

## V. Conclusions

On the basis of a detailed comparison of experimentally measured circularly polarized absorption and emission spectra with calculated spectra based on a Holstein Hamiltonian with spatially correlated site disorder, we have determined that emission in MOPV4 aggregates is mediated by small radius vibrationally dressed excitons (neutral polarons) in which the centrally vibronically excited chromophore is sandwiched between two vibrationally excited neighbors. The center-of-mass of the composite particle is coherently localized over only 2−3 molecules due to the presence of significant disorder. These results illustrate that a quantum mechanical description of electronic excitations in complex molecular architectures, going beyond the Born−Oppenheimer approximation is now feasible. Furthermore, we find that circular polarization is a sensitive probe for delocalization of the excitation and nonadiabatic effects in the electron-vibrational coupling in these chiral systems. The combined theoretical and experimental results indicate that the coherence range for the exciton $N_{\mathrm{coh}}$ and the decay length of the nuclear distortion field $D^{(\mathrm{em})}(r)$ are almost the same, indicating that disorder and EV coupling act synergistically in localizing the exciton to not more than essentially two neighboring molecules, illustrating the intricate nature of photoexcitations in these clusters.

Fluorescent molecular materials are utilized in light-emitting diodes, and the relation between light emission properties and molecular structure is a long-term goal of many research efforts. Our results indicate that both the probability for photon emission and the spectral distribution of the emission ("color") are strongly affected by intermolecular interactions and can only be understood in a proper way by considering the *combined* effect of disorder and EV coupling. Supramolecular systems of $\pi$-conjugated molecules may also be applied as photonic wires and light-harvesting arrays because of the possibility of one-dimensional coherent energy transport over long distances. The results presented here indicate that in the MOPV4 stacks the emitting polarons are confined coherently to only a few repeat units implying that energy transport is dominated by diffusion of such polarons along the stack.[21,41,42] Longer range coherent

(41) Daniel, C.; Herz, L. M.; Silva, C.; Hoeben, F. J. M.; Jonkheijm, P.; Schenning, A. P. H. J.; Meijer, E. W. *Phys Rev. B* **2003**, *68*, 235212−235219.

transport requires a reduction in the *intra*stack disorder or, alternatively, an increase in the spatial correlation length of the excitation energies. The speed at which coherent transport can take place can be improved through the use of molecules that show weak electron-vibration coupling and an example of this design rule are the bacteriochlorophyll molecules in light harvesting systems.[43]

**Acknowledgment.** The work at Temple is supported by the National Science Foundation, grant #DMR-0606028, and Temple University. The work in Mons is partly supported by the Belgian National Fund for Scientific Research (FNRS-FRFC). D.B. is a senior research associate and E.H. is a postdoctoral researcher from FNRS. The research work in Eindhoven was supported by The Netherlands Organization for Scientific Research (NWO) through a grant in the VIDI program. We thank Drs. A. P. H. J. Schenning and P. Jonkheijm for generous supply of the MOPV4 material and their help with the spectroscopic measurements.

**Supporting Information Available:** Detailed experimental procedures for circular polarization measurements in emission. Theoretical expressions for absorption and emission band shape and circular polarization. This material is available free of charge via the Internet at http://pubs.acs.org.

JA067321G

(42) Herz, L. M.; Daniel, C.; Silva, C.; Hoeben, F. J. M.; Schennnig, A. P. H. J.; Meijer, E. W.; Friend, R. H.; Phillips, R. T. *Phys. Rev. B* **2003**, *68*, 045203−045206.
(43) Zazubovich, V.; Tibe, I.; Small, G. J. *J. Phys. Chem. B* **2001**, *105*, 12410−12417.